Materiales de Construcción
Vol. 72, Issue 346, April-June 2022, e283
ISSN-L: 0465-2746
https://doi.org/10.3989/mc.2022.15521

Microscopic observations of sites and forms of ettringite in the microstructure of deteriorated concrete

Y. Ando[a]✉, H. Shinichi[a], T. Katayama[b], K. Torii[c]

a. Taiheiyo Consultant Co. Ltd., (Sakura, Japan)
b. Katayama Petrographic Consulting Office, (Sakura, Japan)
c. Kanazawa Branch, Central Nippon Highway Engineering Nagoya Ltd., (Kanazawa, Japan)
✉: Youko_Andou@taiheiyo-c.co.jp

Received 22 October 2021
Accepted 14 February 2022
Available on line 24 April 2022

ABSTRACT: The determination of delayed ettringite formation (DEF) in hardened concrete relying simply on the identification of ettringite by electron microscopy or powder X-ray diffractometry can be imperfect because of the high risk of missing other possible deterioration phenomena. The presence of ettringite can be easily biased as an indication of DEF while the actual cause of deterioration is ASR. This paper identifies the deterioration causes and presents different ettringite formation factors based on the petrological observation results. The experiments conditions including depth of carbonation, mix proportions of concrete, curing temperature and others were considered. The deterioration of the samples seem to be correlated to ASR, except for the precast concrete product which presented DEF. In order to determine the deterioration causes and demonstrate the importance of petrological approach, different observations using the same methods were carried out on a concrete specimen blended with fly ash showing some cracks.

KEY WORDS: Alkali-silica reaction; Delay-ettringite formation (DEF); Scanning electron microscopy (SEM); Ettringite; Petrography.

Citation/Citar como: Ando, Y.; Shinichi, H.; Katayama, T.; Torii, K. (2022) Microscopic observations of sites and forms of ettringite in the microstructure of deteriorated concrete. Mater. Construcc. 72 [346], e283. https://doi.org/10.3989/mc.2022.15521.

RESUMEN: *Observaciones microscópicas de las posiciones y forma de la etringita dentro de la microestructura del hormigón deteriorado.* La determinación de la formación de la etringita diferida (DEF) en el hormigón endurecido, basado simplemente en la identificación de la etringita a través de microscopía electrónica o difractometría de rayos X en polvo, puede ser imprecisa debido a la alta probabilidad de ignorar otros posibles fenómenos de deterioro. La simple presencia de etringita puede ser fácilmente malinterpretada como una indicación de DEF, mientras que la causa real del deterioro puede deberse a una reacción álcali-sílice (ASR). Este trabajo identifica las causas de deterioro y presenta diferentes factores de formación de etringita basados en los resultados petrográficos, la profundidad de la carbonatación, las proporciones de mezcla del hormigón, la temperatura de curado, y las condiciones ambientales y no ambientales. Se comprobó que el deterioro de las muestras era atribuible al fenómeno de ASR, excepto en el caso del hormigón prefabricado donde se observó el fenómeno de DEF.

PALABRAS CLAVE: Reacción álcali-sílice; Formación de etringita diferida (DEF); Microscopía electrónica de barrido (SEM); Etringita; Petrografía.

This article was selected among the papers presented at the 2022 *International Conference on Alkali-Aggregate Reaction in Concrete* (16th ICAAR)

1. INTRODUCTION

Research of delayed ettringite formation (DEF) has been active in overseas countries (1-5), and recently there have also been some case reports on the phenomenon in Japan (6, 7). There have been two hypotheses proposed about the mechanism of DEF: gaps are produced by the pressure generated from the growth of ettringite crystals (2); or gaps are caused by expansion of cement paste with formation of microcrystalline ettringite (1, 3-5). The latter is strongly supported at present. According to Taylor (1), when DEF is subjected to an early high temperature of 70°C or above during the initial stage of hydration, ettringite decomposes to produce monosulfate, and at the same time, sulfate ions are adsorbed in C-S-H. Then, at ambient temperature, the sulfate ions adsorbed in C-S-H leach out and react with monosulfate to form ettringite, which is thought to exert expansion pressure the nearer it is to the internal hydrate. The coarse ettringite in the gaps and cracks is considered to be a recrystallization precipitate of intrinsically unstable fine ettringite crystals and does not contribute to the expansion.

Ettringite can be detected by electron microscopy within a very small area or powder X-ray diffractometry using finely ground samples, but DEF cannot be judged solely based on the presence of ettringite because there is a high risk of overlooking other possible deterioration phenomena. Ettringite is normally present in concrete and does not necessarily cause expansion (8). However, DEF causes externally visible map cracking in structures, which is similar to alkali silica reaction (ASR). Due to this, when ettringite is present, deterioration actually caused by ASR is often mistaken as caused by DEF (4, 9-11). One factor that leads to this mistake is that ettringite often forms in the cracks caused by ASR (12). For correct determination of DEF or the combined occurrence, petrological analyses are expected to be very useful (4, 9, 13-18). DEF has characteristic features, i.e. gaps around the aggregates and web-like cracks in the paste, both filled with ettringite (3).

The first controversy over whether ASR or DEF was the cause of deterioration occurred in a study of deteriorated precast railroad sleepers in Finland (19, 20). Tepponen and Eriksson (1987), reported that DEF was the cause of deterioration due to heat-treatment, based on scanning electron microscope (SEM) equipped with an energy-dispersive x-ray (EDS). But Shayan and Quick (1992), using SEM/EDS, reported that ASR was the primary cause of damage.

For the highway footings (21-23) in Thailand that showed degradation, ASR was found to be the main factor, but cracks filled with ettringite were observed around the aggregate, and it was debated whether the degradation was combined with DEF. Hirono et al. (2016) (23) conducted an investigation based mainly on polarizing microscopy observations and determined that the cracks around the aggregate were caused by ASR gel flowing out into the weakly interfacial transition zone around the aggregate, and that ASR was the cause of the degradation.

In a study of cracks in prestressed sleepers in India, it was not clear whether the cause of deterioration was ASR or DEF, based only on SEM/EDS using fractured surfaces (24), but polarizing microscopy revealed many cracks filled with ettringite in the cement paste, independent of ASR cracks, and gaps around the aggregate, indicating that combined deterioration of ASR and DEF had occurred (25).

In this study, samples were taken from existing concrete which had cracks under no external sulfate attack and exhibited ettringite formation in the texture. Their deterioration causes were determined by using petrological analyses, and different ettringite formation factors were made clear. An experiment was also carried out using a concrete specimen with cracks after exposure to incineration fly ash, to find the cause of internal deterioration and accompanying expansion due to double salts other than ettringite. The results demonstrated the effectiveness of the petrological approach by means of microstructural observations for such purposes (26).

2. MATERIALS AND METHODS

2.1. Samples used

2.1.1. Concrete with ettringite formation

a) Floor slab with high SO_3 concentration (No. 1); Significant deterioration accompanied with widely distributed cracks is often found in the bottom surface of reinforced concrete (RC) floor slabs of steel bridges aged about 40 years in cold regions with snow cover as shown in Figure 1 (27). These RC slabs are being replaced with those made of prestressed concrete (PC) floor slabs in these several years for the safety of traffic. The sample used in this study was a full depth core (55 mm diameter, 215 mm long) taken from a piece of removed RC slab.

b) Parapet exposed to cold weather (No. 2); The parapet had been placed around a dam lake in an inland mountainous area (Figure 2). The cast in situ concrete was covered with mortar. Numerous cracks with white exudate were found in the side faces of the parapet. Surface concrete has peeled, and white products were also found on the exposed faces. The sample in this study was a fragment of scaling concrete with mortar adhering to it.

c) PC pole with vertical cracks (No. 3); The PC pole in this study was of a tension-type which was required to have a high strength. As shown in Figure 3, two vertical cracks originating from the ground

FIGURE 1: The bottom surface of the floor slab with lattice-like cracks (No. 1).

FIGURE 2: Cracked parapet concrete placed around a dam lake (No. 2), with mortar cover scaling.

FIGURE 3: Vertical cracks in the PC pole (No. 3).

level occurred in the opposing positions in about ten years from the installation. The pole with a nominal strength of 80 N/mm^2, a W/C of 30.5% and a cement content of 525 kg/m^3 had been manufactured by applying centrifugation in a centrifugal casting machine, followed by 4 hours of steam curing at 70°C (28).

d) Precast concrete product with cracks (No. 4); A precast concrete product which had been used outdoors was found to have web-like cracks in the surface. The concrete could have been steam cured during the manufacturing process. The sample was a fragment of concrete taken from the surface area.

2.1.2. Concrete exposed to incineration fly ash (No. 5)

The radioactive substances and other contaminated wastes, generated from the accident at the Fukushima Daiichi Nuclear Power Station and being processed for volume reduction, include incineration fly ash and others with a high content of chlorides. In order to investigate the risk of storing such fly ash in sealed precast containers, an experimental test was performed by filling a real-size concrete container with a paste of incineration fly ash (with addition of $CaCl_2$ and water) and applying the most severe conditions assumed for concrete containers (29). To make observation of concrete easier, a cylindrical specimen (100 mm diameter, 200 mm long) was placed in the precast concrete container filled with fly ash-water mixture with an addition of $CaCl_2$. The mix proportions (water: 150 kg/m^3; cement: 370 kg/m^3; lime based expansive admixture: 25 kg/m^3) and the curing conditions (steam curing for 3 hours at temperatures up to 65°C) used for the cylinder were the same as those of the precast concrete container. The specimen after four months of exposure to fly ash had cracks and scaling in the circumferential surface as shown in Figure 4.

FIGURE 4: Concrete specimen immersed in a paste of incineration fly ash (No. 5).

2.2. Test methods

2.2.1. Polarizing microscopy

Thin section specimens were prepared from the samples, and polarizing microscopy using a polarizing microscope was performed to determine rock types of aggregate, shapes of cracks and occurrence of products.

2.2.2. Electron microscopy

The polished thin sections after the polarizing microscopy were treated by carbon vapor deposition, and scanning electron microscopy was performed by using an electron microscope. Microstructural observation was made with the obtained backscattered electron images (BEI).

2.2.3. EDS quantitative analysis

Some products observed under the polarizing microscope were too fine to identify. In order to identify these products from their compositions, elemental quantitative analysis was performed by energy-dispersive X-ray spectroscopy (EDS) under the electron microscope, and ZAF correction was made to the analysis results. The target elements were SiO_2, TiO_2, Al_2O_3, Fe_2O_3, MnO, MgO, CaO, Na_2O, K_2O, SO_3 and P_2O_5. Chlorine (Cl) was also assayed for the fly ash-exposed concrete sample. EDS mapping of SO_3 was performed for the floor slab sample.

3. RESULTS AND DISCUSSION

3.1. Concrete with ettringite formation

3.1.1. Polarizing microscopy

a) Floor slab with high SO_3 concentration (No. 1); Aggregate consisted of gravel and sand mainly comprised of granite, diorite, rhyolitic welded tuff and andesite. ASR cracks were found extending from aggregate particles of andesite, rhyolite or rhyolitic welded tuff into the cement paste (Figure 5a). The depth of carbonation was 20 mm in the bottom surface, while being 3 mm in the top surface which had been in contact with the asphalt.

b) Parapet exposed to cold weather (No. 2); Aggregate consisted of gravel and sand mainly comprised of siliceous shale, shale, sandstone and andesite. ASR cracks were found extending from the aggregate particles of andesite into the cement paste, and needle-like crystals were observed to fill the cracks in the cement paste (Figure 5b). Several parallel cracks and scaling were found in the concrete surface immediately below the mortar cover, with needle-like crystals filling the cracks (Figure 5c). No entrained air voids were found in the cement paste.

c) PC pole with vertical cracks (No. 3); In the PC pole manufactured by centrifugal casting, a larger amount of coarse aggregate was present near the surface, and larger amounts of fine aggregate and cement were present in the inside. The coarse aggregate was gravel mainly comprised of diorite, granite, gabbro, gneiss and rhyolitic welded tuff, and the fine aggregate was sand mainly comprised of rhyolitic welded tuff, granitic rocks and andesite. ASR was found around the coarse aggregate particles of rhyolitic welded tuff near the surface of the pole (Figure 5d), and around the fine aggregate particles of andesite in the inside (Figure 5e). ASR was more significant in the inside of the pole where the andesite content was higher. In the inside, ASR cracks were propagating into the cement paste, and they were filled with needle-like crystals that formed

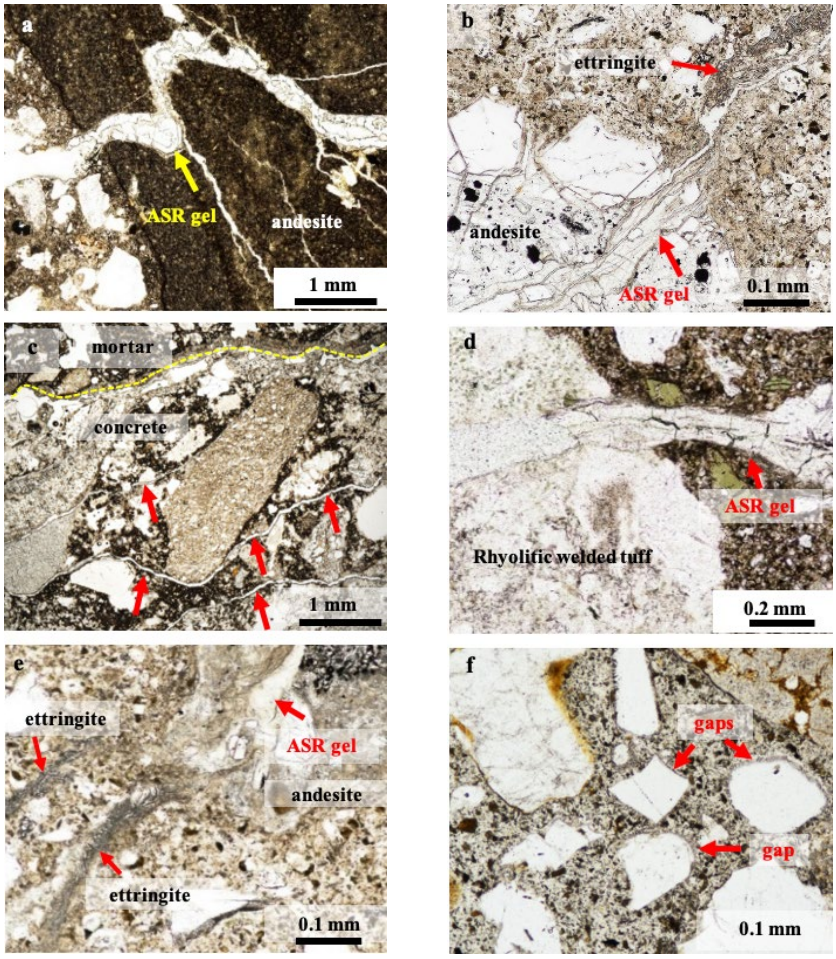

FIGURE 5: Polarizing microscopic images: (a) cracks originating from andesite (No. 1); (b) cracks in andesite filled with ASR gel, and cracks in the cement paste filled with ettringite (No. 2); (c) parallel cracks (red arrows) under the mortar cover (No. 2); (d) cracks filled with ASR gel near the surface of the PC pole (No. 3); (e) cracks filled with ettringite inside the pole (No. 3); (f) needle-like crystals filling the gaps between aggregate particles and cement paste (No. 4).

to replace the ASR gels (Figure 5e). Most of the ASR cracks developed concentrically parallel to the circumference of the pole, but some cracks without products were also found growing in the direction perpendicular to them.

d) Precast concrete product (No. 4); Coarse aggregate consisted mainly of crushed stone of sandstone and shale, and fine aggregate was sand comprised of granite-derived crystalline and rock fragments. No ASR was observed in the concrete under the polar-

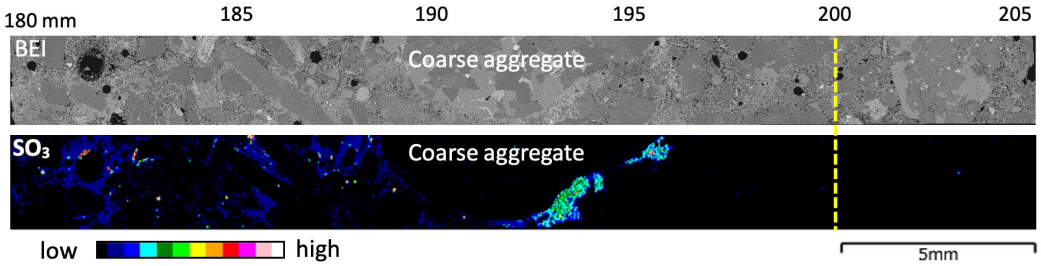

FIGURE 6: Elemental mapping of the SO_3 rich area by EDS (No. 1). The numbers represent the depths from the slab top surface. The carbonation area in the bottom surface is on the right side of the dotted line.

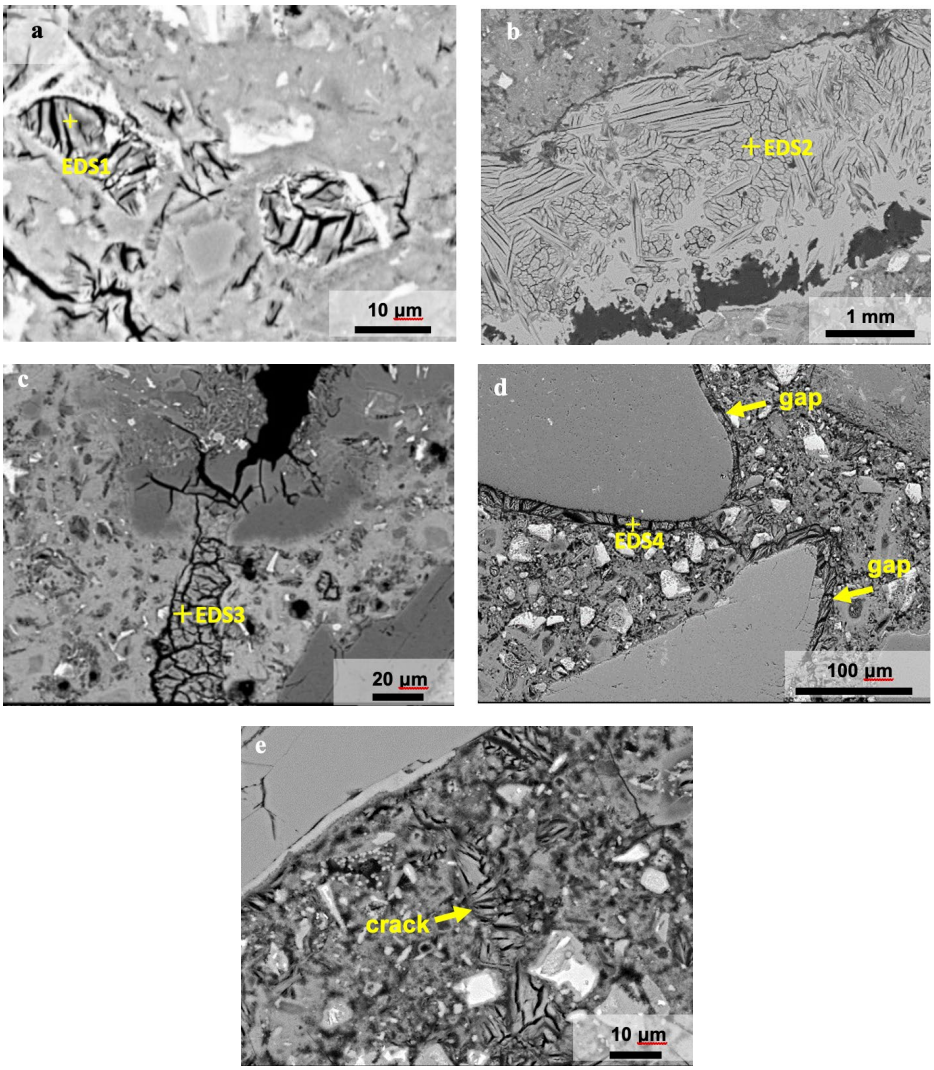

FIGURE 7: BEI of the thin sections: (a) ettringite within the cement paste with a high SO_3 concentration (No. 1); (b) ettringite filling the cracks (No. 2); (c) cracks filled with ettringite (No. 3); (d) gaps generated between aggregate particles and cement paste (No. 4); (e) ettringite filling the cracks in the cement paste (No. 4).

izing microscope, while there were gaps filled with needle-like crystals between aggregate particles and cement paste (Figure 5f).

3.1.2. Electron microscopy

a) Floor slab with high SO_3 concentration (No. 1); Figure 6 shows an EDS map of SO_3 in the bottom surface of the slab. High concentrations of SO_3 were found at around 180 to 195 mm from the top surface of the slab, with some variations due to the inhomogeneity within the observation area where cement paste and aggregate particles were present. No cracks were found in this area. Cement hydrates were found to have needle- or plate-like crystals at the center, and formation of ettringite (Figure 7a) was confirmed by the EDS analysis (Table 1).

The ideal composition formula of ettringite is $3CaO, Al_2O_3, 3CaSO_4, 32H_2O$ (CaO: 26.81%, Al_2O_3: 8.12%, SO_3: 19.14%, H_2O: 45.93%), and the total EDS analysis value is low due to the presence of bound water. Since some of the bound water in ettringite undergoes dehydration in the electron microscope, a high vacuum condition, the total of $CaO+A_{l2}O_3+SO_3$ is 54.07% in the ideal equation, but the actual total analysis value of the three elements is as high as 72%.

b) Parapet exposed to cold weather (No. 2); The needle-like crystals filling the cracks caused by scaling were confirmed to be ettringite by the SEM observation (Figure 7b) and EDS analysis (Table 1). Ettringite was also found in the cracks caused by ASR in the cement paste.

c) PC pole with vertical cracks (No. 3); The needle-like crystals (Figure 7c) were observed in the form of cross section of their slices under the electron microscope, and they were confirmed to be ettringite by the EDS analysis (Table 1).

d) Precast concrete product (No. 4); Numerous fine cracks (Figure 7d, 7e) were observed in the cement paste under the electron microscope. Needle-like crystals were found filling the fine cracks as well as the gaps between aggregate particles and the cement paste, and they were confirmed to be ettringite by the EDS analysis (Table 1).

3.2. Fly ash-exposed concrete

3.2.1. Polarizing microscopy

Cracks and scaling were found along the circumference near the surface of the specimen as shown in Figure 8a. The cracks were extending along the peripheries of aggregate particles into the cement

Table 1: Results of EDS analysis (%).

	No.1	No.2	No.3	No.4		No.1	No.2	No.3	No.4
SiO_2	2.51	5.94	1.45	0.77	Ca	5.28	4.92	5.67	5.76
TiO_2	0.00	0.04	0.00	0.13	Mn	0.00	0.00	0.00	0.00
Al_2O_3	11.38	9.98	10.96	10.00	Mg	0.07	0.02	0.00	0.01
Fe_2O_3	0.09	0.00	0.00	0.17	Na	0.04	0.00	0.00	0.01
MnO	0.00	0.00	0.00	0.00	K	0.01	0.00	0.00	0.02
MgO	0.33	0.08	0.00	0.04		5.40	4.94	5.67	5.80
CaO	34.35	33.46	35.37	32.80	Si	0.36	0.82	0.22	0.13
Na_2O	0.20	0.00	0.00	0.03	Ti	0.00	0.00	0.00	0.02
K_2O	0.07	0.01	0.00	0.08	Al	1.93	1.61	1.93	1.93
SO_3	26.57	21.73	26.40	22.43	Fe	0.01	0.00	0.00	0.02
P_2O_5	0.04	0.00	0.00	0.00		2.29	2.43	2.15	2.10
Cl	0.00	0.00	0.00	0.00	T. cation	7.70	7.37	7.82	7.89
Total	75.54	71.24	74.18	66.45	O	9	9	9	9
					S	2.86	2.24	2.96	2.76
					P	0.00	0.00	0.00	0.00
					2Cl	0.00	0.00	0.00	0.00
						2.86	2.24	2.96	2.76

Standardized formulae with theoretical values of the minerals:
EDS 1: ettringite $(Ca_{5.28}, Na_{0.04}, K_{0.01}, Mg_{0.07})_{5.40}\ (Al_{1.93}, Si_{0.36}, Fe_{0.01})_{2.29}\ O_6\ (SO_4)_{2.86}\bullet nH_2O$
EDS 2: ettringite $(Ca_{4.92}, Mg_{0.02})_{4.94}\ (Al_{1.61}, Si_{0.82})_{2.43}\ O_6\ (SO_4)_{2.24}\bullet nH_2O$
EDS 3: ettringite $Ca_{5.67}\ (Al_{1.93}, Si_{0.22})_{2.15}\ O_6\ (SO_4)_{2.96}\bullet nH_2O$
EDS 4: ettringite $(Ca_{5.76}, Na_{0.01}, K_{0.02}, Mg_{0.01})_{5.80}\ (Al_{1.93}, Si_{0.13}, Ti_{0.02,}\ Fe_{0.02})_{2.29}\ O_6\ (SO_4)_{2.76}\bullet nH_2O$

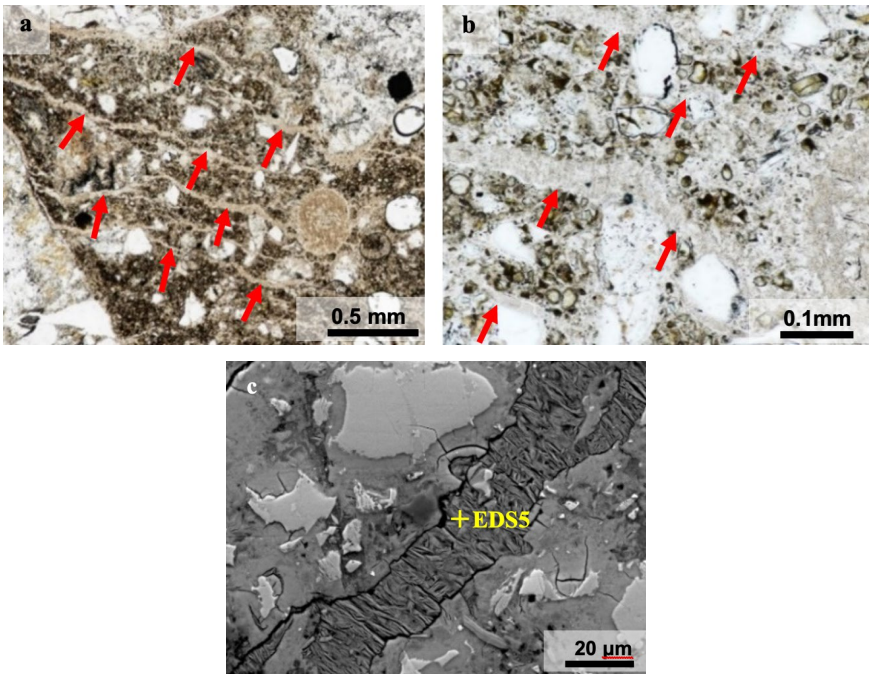

FIGURE 8: Microscopic images (No. 5): (a) parallel cracks (red arrows) near the core surface; (b) needle-like crystals filling the cracks (red arrows); (c) 3-1-15 crystalline phase in the crack. (a, b: plane polarized light; c: BEI).

TABLE 2: Results of EDS analysis (%).

	No.5		No.5
SiO_2	0.32	Ca	3.85
TiO_2	0.23	Mg	0.01
Al_2O_3	0.1	Na	0.00
Fe_2O_3	0.38	K	0.01
MnO	0	Si	0.03
MgO	0.1	Ti	0.01
CaO	42.13	Al	0.01
Na_2O	0.04	Fe	0.02
K_2O	0.05	Mn	0.00
SO_3	0.21	T. cation	3.95
P_2O_5	0.00	O	4
Cl	12.65	S	0.01
*-O=2C1	2.85	P	0.00
Total	53.36	2Cl	0.91
* -O=2Cl (0.2256xCl)			
Standardized formula with theoretical values of the minerals: EDS 5: 3-1-15 crystalline phase ($Ca_{3.85}$, $K_{0.01}$, $Mg_{0.01}$, $Al_{0.01}$, $Si_{0.03}$, $Ti_{0.01,}$ $Fe_{0.02}$)$_{3.95}$ O_3 $2(Cl)_{0.91}$•nH_2O			

paste. These surface cracks were observed within a depth range of about 3 mm from the circumferential surface of the specimen. Needle-like crystals were found to be present in the cracks under the polarizing microscope (Figure 8b). No ASR was confirmed.

3.2.2. Electron microscopy

The needle-like crystals in the cracks were found to intersect at almost right angles each other under the electron microscope (Figure 8c). Its composition was confirmed to be $3CaO•CaCl_2•15H_2O$ by the EDS analysis (Table 2). The total EDS analysis value of $3CaO•CaCl_2•15H_2O$ is low due to the presence of water. Like ettringite, some of the bound water in $3CaO•CaCl_2•15H_2O$ undergoes dehydration in the electron microscope, then the actual analysis value becomes a little higher than the ideal total of $CaO+CaCl_2$ in the ideal equation, which is 50.8%.

4. DISCUSSION

4.1. Estimated deterioration causes and discussion

Excluding the precast concrete product (No. 4), all of the floor slab (No. 1), the parapet (No. 2) and the PC pole (No. 3) had ASR cracks extending from aggregate particles into the cement paste. Ettringite formation was confirmed in all of the four samples, but none of them had been exposed to external sulfate attack.

No cracks were found in the SO_3 rich area in the floor slab (No. 1). Considering the depth of carbonation, it was likely that sulfate ions were formed during decomposition of ettringite in the carbonation area, eluted into the pore solution, carried to the inside due to concentration diffusion and concentrated

there, then used to form ettringite (30). Therefore, the main cause of the deterioration is thought to be ASR.

The cause of the cracks in the parapet exposed to cold weather (No. 2) was ASR. The scaling of the mortar cover can be attributed to frost attack. One reason is the absence of entrained air voids in the cement paste. The sample, which had been exposed to freezing and thawing actions during the winter, had laminar cracks parallel to the surface where scaling was found. These suggested that the ettringite did not contribute to formation of cracks, but precipitated from the soluble components which had leached into the cracks due to the freezing and thawing actions. In deteriorated concretes the formation of ettringite is promoted by the migration of the soluble sulfates from inside the concrete toward the external surface (30).

There was a concern of DEF for the PC pole (No. 3) which had been steam cured at high temperatures. However, observation showed no characteristic findings of DEF, i.e. gaps between aggregate particles and the cement paste, and web-like cracks in the cement paste (9). The cracks filled only with ASR products were likely to have occurred due to a large tensile stress acting on the concrete surface as a result of ASR expansion of concrete. Formation of ettringite was found in cracks that were obviously attributable to ASR, which suggested no association with expansion. Replacement of ASR gel by ettringite, leaving a texture of original ASR gel within cracks, has been reported (31). One of the possible factors of ettringite formation was considered to be the high SO_3 concentration which was originally high due to the high cement content in the concrete mix proportions and further increased in the inside by the centrifugal casting. The other possible factor was the water which could enter from the ASR cracks and promoted re-formation of ettringite (12, 32).

The precast concrete product (No. 4) had been used in an area with no influence of freezing and thawing actions, and thus frost attack was excluded from possible causes. Ettringite was found all over the concrete sample, which also excluded the possibility of the concentration diffusion carrying the SO_3 from the carbonation area. The precast concrete product could have been steam cured during the manufacturing process, and the polarizing and electron microscopic observations revealed the presence of gaps between aggregate particles and the cement paste, as well as fine cracks in the cement paste, and both of which were found filled with ettringite. Consequently, DEF was highly likely to be the cause of deterioration.

4.1.2. Deterioration causes of the incineration fly ash-exposed concrete

As one of the concrete deterioration phenomena caused by deicing salt, chemical deterioration is known to occur in concrete immersed in a highly concentrated solution of $CaCl_2$ of 30°C or below, being accelerated by the action of dry and wet cycles (33). One of the possibilities for the deterioration of concrete is the leaching of $Ca(OH)_2$ from cement paste making the paste porous (29). The other possibilities is the crystal growth pressure caused by the formation of $3CaO•CaCl_2•15H_2O$ (hereafter, the 3-1-15 crystalline phase), which is formed by the reaction of Equation [1] (18):

$$3Ca(OH)_2 + CaCl_2 + 15H_2O \rightarrow 3CaO•CaCl_2•15H_2O \quad [1]$$

The 3-1-15 crystalline phase is considered to result in volumetric expansion to about two times $Ca(OH)_2$, pressure of which acts on the hardened concrete and ultimately causes expansion failure (33).

Reported strain of the precast container indicated expansion in winter and overall contraction in other seasons (33). Therefore, the reason of the parallel cracks at the concrete surface can be attributed to frost attack due to the freezing and thawing and combined formation of the 3-1-15 crystalline phase within cracks.

4.2. Importance of microstructural observation using microscopes

Ettringite and the 3-1-15 crystalline phase are double salts which are formed in concrete containing $Ca(OH)_2$, and both can cause deterioration of the concrete. Similar to ASR, formation of $3CaO•CaCl_2•15H_2O$ directly causes volumetric expansion and concrete deterioration, and The substance causing the expansion can be clearly observed. By contrast, in DEF which occurs upon supply of moisture after exposure to elevated temperatures, concrete expansion is caused by secondary ettringite which is formed in the cement paste. The secondary ettringite is so fine and unstable (1) that it cannot be observed in the magnification ranges of polarizing or electron microscopes. What is actually observed microscopically is considered to be the ettringite that has formed by solution and re-precipitation in cracks or gaps between aggregate particles and cement paste caused by expansion of cement paste (1), and trace of which is the determining factor of DEF in the microstructure observation. Therefore, it is inappropriate to make judgement on DEF, without microstructural observation, based only on detection of ettringite by electron microscopy and EDS analysis in a microscopic area of concrete or by powder X-ray diffractometry using finely ground samples. The microstructure observation in a wider view by polarizing microscopy is essential to determination of concrete deterioration causes, and its combined use with electron microscopy and EDS analysis is

important for examining fine cracks and locating and assaying the products.

It has been known that factors that contribute to stable formation of ettringite include temperatures and alkali ion concentration, and that ettringite decomposes to produce monosulfate at elevated temperatures and at high alkali ion concentrations (34). For the estimation of ettringite formation factors, it is necessary to make comprehensive consideration with the depth of carbonation, concrete mix proportions, curing conditions and various environmental conditions taken into account.

5. CONCLUSIONS

In this study, causes of deterioration of several samples concrete with cracks, produced under no external sulfate attack and exhibiting ettringite formation in the texture were determined. Authors claim the microstructure observation by polarizing microscopy as an essential step to determination of concrete deterioration causes, and its combined use with electron microscopy and EDS analysis, that is important for examining fine cracks and locating and assaying the products. They find also important in determining DEF, take into account the occurrence of previous damage due to ASR and frost attack. There is no such collection and presentation of cases that can be easily misinterpreted as DEF, and the importance of determining DEF after confirming degradation phenomena other than DEF was demonstrated. In addition, we raised awareness of the fact that DEF is easily determined.

ACKNOWLEDGEMENTS

The authors would like to thank Associate Professor Yoshimori Kubo of Kanazawa University, Dr. Masahiro Nomura of Nomura Concrete Laboratory Co., Ltd., and Mr. Hiroaki Mori of Taiheiyo Cement Corporation for their advices regarding this research.

AUTHOR CONTRIBUTIONS:

Conceptualization: Y. Ando. Data curation: Y. Ando, H. Shinichi. Formal analysis: Y. Ando, J. Smith. Methodology: T. Katayama. Validation: H. Shinichi, T. Katayama. Visualization: Y. Ando. Writing, original draft: Y. Ando, H. Shinichi, T. Katayama, K. Torii. Writing, review & editing: T. Katayama, K. Torii.

REFERENCES

1. Taylor, H.F.W.; Famy, C.; Scrivener, K.L. (2001) Delayed ettringite formation. *Cem. Concr. Res.* 31 [5], 683-693. https://doi.org/10.1016/S0008-8846(01)00466-5.
2. Heinz, D.; Ludwig, U. (1987) Mechanism of secondary ettringite formation in mortars and concretes subjected to heat treatment. Concrete durability. *ACI SP-100*. 2, 2059-2071.
3. Scrivener, K.L.; Taylor, H.F.W. (1993) Delayed ettringite formation: A microstructural and microanalytical study. *Adv. Cem. Res.* 5 [20], 139-146. https://doi.org/10.1680/adcr.1993.5.20.139.
4. Johansen, V.; Thaulow, J.; Skalny, J. (1993) Simultaneous presence of alkali-silica gel and ettringite in concrete. *Adv. Cem. Res.* 5 [17], 23-29. https://doi.org/10.1680/adcr.1993.5.17.23.
5. Shimada, Y.; Vagn, C.; Johansen, F.; MacGregor, M.; Thomas, O. (2005) Chemical path of ettringite formation in heat-cured mortar and its relationship to expansion: A literature review. *PCA Res. Dev. Bul.* RD136.
6. Kawabata, Y. (2018) Diagnosis on expansion of heat-cured precast concrete blocks due to delayed ettringite formation in Japan. 6th ICDCS. 516-524.
7. Fujikane, M.; Nakahara, K.; Nakamura, T. (2009) A report about the deterioration of the concrete product by delayed ettringite formation (DEF). *Civil Eng. J.* 51 [11], 38-41. (in Japanese)
8. Poole, A.B.; Ian, S. (2016) Concrete Petrography. *CRC Press.* 420. https://doi.org/10.1201/b18688.
9. Thomas, M.D.A.; Folliard, K.; Drimalas, T.; Ramlochan, T. (2008) Diagnosing delayed ettringite formation in concrete structures. *Cem. Conc. Res.* 38 [6], 841-847. https://doi.org/10.1016/j.cemconres.2008.01.003.
10. Shayan, A.; Quick, G.W. (1992) Microscopic features of cracked and uncracked concrete railways sleepers. *ACI Mater. J.* 89, 348-364.
11. Larive, C.; Louarn, N. (1992) Diagnosis of alkali-aggregate reaction and sulphate reaction in French structures. Proce. 9th ICAAR. 587-598.
12. Shayan, A.; Quick, G.W. (1992) Relative importance of deleterious reactions in concrete: formation of AAR products and secondary ettringite. *Adv. Cem. Res.* 4 [16], 149-157. https://doi.org/10.1680/adcr.1992.4.16.149.
13. Hime, W.G.; Marusin, S.; Jugovic, Z.; Martinek, R.; Cechner, R.; Backus, L. (2000) Chemical and petrographic analyses and ASTM test procedures for the study of delayed ettringite formation. *Cem. Conc. Agg.* 22 [2], 160-168.
14. Skalny, J.; Johansen, V.; Thoulow, N.; Palomo, A. (1996) DEF: As a form of sulfate attack. *Mater. Construcc.* 46 [244], 5-29. https://doi.org/10.3989/mc.1996.v46.i244.519.
15. Marusin, S.L. (1993) SEM studies of DEF in hardened concrete. Proc. 15th ICCM, *Dallas*. 289-299.
16. Marusin, S.L. (1994) A Simple treatment to distinguish alkali-silica gel from delayed ettringite formations in concrete. *Mag. Conc. Res.* 46 [168], 163-166. https://doi.org/10.1680/macr.1994.46.168.163.
17. João, C.; António, B.R. (2019) Evaluation of damage in concrete from structures affected by internal swelling reactions – A case study. *Procedia Stru. Integ.* 17, 80-89. https://doi.org/10.1016/j.prostr.2019.08.012.
18. Owsiak, Z. (2010) The effect of delayed ettringite formation and alkali-silica reaction on concrete microstructure. *Ceramics Silikaty.* 54 [3], 277-283. https://doi.org/10.1016/j.prostr.2019.08.012. Retrieved from https://www.irsm.cas.cz/materialy/cs_content/2010/Owsiak_CS_2010_0000.pdf.
19. Tepponen, P.; Eriksson, B.E. (1987) Damage in concrete railway sleepers in Finland. *Nordic Conc. Res.* 6, 199-209.
20. Shayan, A.; Quick, G.W. (1994) Alkali-aggregate reaction in concrete railway sleepers from Finland. Proc. 16th International Conference on cement microscopy. 69-79.
21. Jensen, V.; Sujjavanich, S. (2016) ASR and DEF in concrete foundations in Thailand. Proc. 15th ICAAR, Sao Paulo, Brazil.
22. Jensen, V.; Sujjavanich, S. (2016) Alkali silica reaction in concrete foundation in Thailand. Proc. 15th ICAAR, Sao Paulo, Brazil.
23. Hirono, S.; Yamada, K.; Ando, Y.; Sato, T.; Yamada; K.; Kagimoto, H.; Torii, K. (2016) ASR found in Thailand and tropical regions of southeast asia. Proc. 15th ICAAR, Sao Paulo, Brazil.
24. Awasthi, A.; Matsumoto, K.; Nagai, K.; Asamoto, S.; Goto, S. (2017) Investigation on possible causes of expansion

damages in concrete – a case study of sleepers in Indian Railways. *J. Asian Conc. Fed. 3* [1], 49-66.
25. Ando, Y.; Katayama, T.; Asamoto, S.; Nagai, K. (2018) Investigation to determine the causes of the cracks occurred in the PC sleepers of Indian railways and interaction of ASR and DEF. *Proc. JCI Annual Convention.* 40 [2], 909-914. (in Japanese). Retrieved from http://data.jci-net.or.jp/data_html/40/040-01-1146.html.
26. Ando, Y.; Hirono, S.; Katayama, Y.; Torii, K. (2018) Microscopic observation of sites and forms of ettringite in the microstructure of deteriorated concrete. *Cem. Sci. Conc. Tec.* 72 [1], 2-9. (in Japanese). https://doi.org/10.14250/cement.72.2.
27. Nomura, M.; Ura, S.; Ishii, K.; Torii, K. (2017) Influence of hot asphalt paving on steel bridge reinforced concrete slabs and detailed analysis on cores from real structures. *Proc. JCI Annual Convention.* 39 [1], 931-936. (in Japanese).
28. Hashimoto, T.; Kanai, S.; Hirono, S.; Torii, K. (2015) A consideration on improvement in durability aspects of concrete poles. *Cem. Sci. Conc. Tec.* 69 [1], 550-557. (in Japanese) https://doi.org/10.14250/cement.69.550.
29. Mori, H.; Yamada, K.; Iwaki, I.; Nagataki, S. (2018) Demonstration experiment on durability of concrete containers storing incineration fly ash contaminated with radionuclides and technical requirements of such containers. *Conc. J.* 56 [4], 296-303. (in Japanese). Retrieved from https://www.jstage.jst.go.jp/article/coj/56/4/56_296/_article/-char/ja/.
30. Durand, B.; Marchand, B.; Larivere, R.; Bergeron, J.M.; Pelletier, G.; Ouimet, M.; Berard, J.; Katayama, T. (2004) A special history case about severe damages due to freezing and thawing combined with sulfate migration and ASR at Rapides-Des-Quinze hydraulic structures. Proc. 12th ICAAR.
31. Jones, T.N.; Poole, A.B. (1986) Alkali-silica reaction in several U.K. concretes: The effect of temperature and humidity on expansion, and the significance of ettringite development. Proc. 7th ICAAR. 446-451.
32. Shayan, A.; Ivanusec, I. (1996) An experimental clarification of the association of delayed ettringite formation with alkali aggregate reaction. *Cem. Conc. Comp.* 18 [3], 161-170. https://doi.org/10.1016/0958-9465(96)00012-1.
33. Chatterji, S. (1978) Mechanism of the $CaCl_2$ attack on Portland cement concrete. *Cem. Concr. Res.* 8 [4], 461-467. https://doi.org/10.1016/0008-8846(78)90026-1.
34. Michaud, V.; Sorrentino, D. (2003) Influence of temperature and alkali concentration on thermodynamical stability of sulphoaluminate phases. Proc. 11th ICCC. 2033-2043.